1 # Significant contribution of organics to aerosol liquid water content in

2 # winter in Beijing, China

5 **Xiaoai Jin[1], Yuying Wang[1,2], Zhanqing Li[3], Fang Zhang[1], Weiqi Xu[4,5], Yele Sun[4,5], Xinxin Fan[1],**

6 **Guangyu Chen[6], Hao Wu[1], Jingye Ren[1], Qiuyan Wang[2], and Maureen Cribb[3]**

9 [1]State Key Laboratory of Earth Surface Processes and Resource Ecology, College of Global Change and Earth System

10 Science, Beijing Normal University, Beijing 100875, China

11 [2]School of Atmospheric Physics, Nanjing University of Information Science and Technology, Nanjing 210044, Chi

12 na

13 [3]Department of Atmospheric and Oceanic Science, and Earth System Science Interdisciplinary Center, University of

14 Maryland, College Park, MD, USA

15 [4]State Key Laboratory of Atmospheric Boundary Layer Physics and Atmospheric Chemistry, Institute of Atmospheric

16 Physics, Chinese Academy of Sciences, Beijing 100029, China

17 [5]College of Earth Sciences, University of Chinese Academy of Sciences, Beijing 100049, China

18 [6]Faculty of Geographical Science, Beijing Normal University, Beijing 100875, China

20 Correspondence to: Zhanqing Li (zli@atmos.umd.edu), Yuying Wang (wyy_bnu@126.com)

26 **Abstract**

28 The aerosol liquid water content (ALWC), an important component of atmospheric particles, has a

29 significant effect on atmospheric optical properties, visibility and multiphase chemical reactions. In

30 this study, ALWC is determined from aerosol hygroscopic growth factor and particle number size

31 distribution (PNSD) measurements and also simulated by the ISORROPIA II thermodynamic model

32 with measured aerosol chemical composition data at an urban site in Beijing from 8 November to 15

33 December 2017. Rich measurements made during the experiment concerning virtually all aerosol

34 properties allow us not only to derive the ALWC but also to study the contributions by various species

35 for which little has been done in this region. The simulated ALWC including the contribution of

36 organics and the calculated ALWC are highly correlated (coefficient of determination $R^2 = 0.92$). The

37 ALWC contributed by organics ($ALWC_{Org}$) accounts for 30 % ± 22 % of the total ALWC during the

38 sampling period. These results suggest a significant contribution of organics to ALWC, which is rather

39 different from previous studies that showed negligible contributions by organics. Our results also show

40 that ALWC correlates well with the mass concentrations of sulfate, nitrate, and secondary organic

41 aerosols (SOA) ($R^2 = 0.66$, 0.56, and 0.60, respectively). We further noted that accumulation mode

42 particles play a key role in determining ALWC, dominating among all the aerosol modes. ALWC is an

43 exponential function of ambient relative humidity (RH) whose strong diurnal variation influence the

44 diurnal variation of ALWC. However, there is a three-hour lag between the extremes of ALWC and

45 RH values, due to the diurnal variations in PNSD and aerosol chemical composition. Finally, a case

46 study reveals that $ALWC_{Org}$ plays an important role in the formation of secondary aerosols through

47 multiphase reactions at the initial stage of a heavy haze episode.

48

49

50

1. Introduction

China has experienced rapid economic developments during the past few decades, resulting in frequent heavy haze events. Severe air pollution may harm human health and affect the regional climate through aerosol direct and indirect radiation effects (Li et al., 2016; G. X. Wu et al., 2016). However, air pollution formation mechanisms and aerosol climate effects remain highly uncertain due to the complex physical and chemical processes involved (Tao et al., 2012; Y. Wang et al., 2014).

Aerosol liquid water (ALW), a component of atmospheric particles in the atmosphere, exists universally and plays an important role in many atmospheric physical and chemical processes (Nguyen et al., 2016). For example, ALW can influences aerosol optical properties, resulting in increased extinction coefficients, lowered atmospheric visibilities, enhanced aerosol optical depths (AODs), and changes in the direct climatic effect of aerosols (Dougle et al., 1996; Adams et al., 2001; Liao et al., 2005; Seinfeld and Pandis, 2006). Secondary aerosols (SA) are considered to be the main source of particulate pollution during heavy haze events in China (Huang et al., 2014). Many studies now highlight the significance of aerosol liquid water content (ALWC) in the formation of SA through chemical reactions (e.g., Arellanes et al., 2006; G. Wang et al., 2016; Cheng et al., 2016). This is because ALW can dilute the absolute concentration of solutes, adjust aerosol acidity, and serve as a reactant, resulting in increases in trace gas (e.g., N_2O_5 and HO_2) uptake coefficients (Wahner et al., 1998; Bertram et al., 2009; Abbatt et al., 2012). H. Wang et al. (2017) found that the uptake coefficient of N_2O_5 can be high, which is related to high ALWC in Beijing, thereby increasing the formation of nitrates. ALW can also speed up the aqueous phase chemical reaction by serving as a reactor for the transformation of SO_2 to sulfate (Zheng et al., 2015; G. Wang et al., 2016; Cheng et al., 2016). Some studies have found that ALWC can facilitate the formation of secondary organic aerosols (SOA) through aqueous-phase chemistry and photochemistry (Blando et al., 2001; Surratt et al., 2007; Hennigan et al., 2008; Song et al., 2019). Furthermore, observations in Beijing have shown that aqueous-phase processes play a dominant role in the additional formation of oxidized SOA (Xu et al.,

76   2017). Overall, investigating the formation of SA and haze in North China requires an examination of

77   ALWC and its factors in this region.

78   However, directly measuring real-time ALWC is difficult because of technical limitations,

79   especially under high RH conditions (Kuang et al., 2018). Four indirect methods have been proposed

80   to calculate real-time ALWC: (1) the aerosol particle number size distribution (PNSD) under dry

81   conditions and ambient relative humidity (RH) conditions are first measured, then ALWC is calculated

82   as the difference between dry and ambient aerosol volumes (Stanier et al., 2004); (2) the increased

83   aerosol volume due to water uptake (i.e., ALWC) is calculated according to the measured dry PNSD,

84   size-dependent aerosol hygroscopicity, and ambient RH (Kitamori et al., 2009; Bian et al., 2014; Tan

85   et al., 2017); (3) the dry and ambient aerosol volumes are first estimated using the measured aerosol

86   optical enhancement and Ångström exponent, then ALWC is calculated as the difference between dry

87   and ambient aerosol volumes (Kuang et al., 2018); and (4) ALWC is simulated using thermal

88   equilibrium models such as the ISORROPIA thermodynamic model (Nenes et al., 1998), Aerosol

89   Inorganics Model models (Wexler and Clegg, 2002), the Simulating Composition of Atmospheric

90   Particles in Equilibrium model (Kim et al., 1993), and the Gibb's Free Energy Minimization model

91   (Ansari et al., 1999) with aerosol chemical composition information as input.

92   ALWC mostly depends on aerosol PNSD, chemical composition, and ambient RH. Hodas et al.

93   (2014) reported that ALWC in the Po Valley in Italy is driven by locally formed anthropogenic nitrates.

94   The implications for the lifetimes of water-soluble organic compounds and its potential influence on

95   SOA formation were also discussed. Another study also revealed that ALWC in Beijing was driven by

96   secondary inorganic aerosols (SIA; Z. Wu et al., 2018). Most previous studies have focused on the

97   interaction between inorganic salts and ALWC, but the impact of organic species on ALWC been

98   ignored to our knowledge (Blando et al., 2001; Surratt et al., 2007; Hennigan et al., 2008; Carlton et

99   al., 2014). A thorough understanding of the association of ALWC with organic aerosols in the

100   atmosphere is lacking.

101 In this study, ALWC is calculated using the indirect method (2) and simulated using the

102 ISORROPIA II model, i.e., indirect method (4), discussed previously. The effects of inorganic aerosols,

103 organic aerosols, PNSD, and ambient RH on ALWC are then investigated separately. We demonstrate

104 the significant contribution of organics to ALWC in Beijing and provide evidence that the ALW

105 contributed by organics serves as a reactor for sulfate and SOA formation.

106 **2. Data and measurements**

107 **2.1. Sampling site**

108 The Air Pollution and Human Health (APHH) winter field campaign took place from 8 November

109 to 15 December 2016 at the Chinese Academy of Sciences' Institute of Atmospheric Physics Tower

110 Branch in Beijing. Beijing is located in the northwest part of the North China Plain, which has

111 experienced rapid economic developments during the last few decades. A large amount of gaseous

112 precursors and other air pollutants are emitted in this region every year, causing serious air pollution

113 problems. The sampling site is located in the northwestern urban area of Beijing (39.97°N, 116.37°E),

114 between the north third and fourth ring roads and surrounded by restaurants. Traffic and cooking

115 emissions are thus the main pollutants at the site. Aerosols at this site can, therefore, well represent

116 anthropogenic aerosols in highly polluted areas. Sun et al. (2013) and Y. Wang et al. (2017) provide

117 more detailed descriptions of the sampling site.

118 **2.2. Instrumentation**

119 Sampling instruments used during the field campaign included a scanning mobility particle sizer

120 (SMPS) equipped with a long differential mobility analyzer (DMA; model 3081A, TSI) and a

121 condensation particle counter (CPC; model 3772, TSI). A custom-built hygroscopicity tandem

122 differential mobility analyzer (H-TDMA) was installed in an air-conditioned mobile container at

123 ground level. The temperature inside the container was maintained at 20–25°C. A high-resolution

124   aerosol mass spectrometer (HR-AMS) was set up in a sampling room located on a two-story roof,

125   about 25 m north from the container. Sampled air went through a $PM_{2.5}$ cyclone inlet fixed on the top

126   of the container before entering the instruments. The RH of the sampled air was dried to below 20 %

127   by a dryer system consisting of a tube filled with silica gel and a Nafion dryer (model PD-70T-24ss,

128   Perma Pure Inc., USA). Various meteorological parameters, including wind speed (WS), wind

129   direction (WD), temperature (T), and RH, were measured from a 325-m meteorological tower located

130   ~20 m west of the container. In this study, all times are reported in Beijing local time (UTC+8 h).

131   PNSDs with electrical-mobility diameters ranging from 10 to 600 nm were measured by a

132   scanning mobility particle sizer (SMPS) at a 5-min time resolution. PNSDs were extended to diameters

133   ranging from 0.6 to 1 μm by fitting the measured PNSDs with functions consisting of three-mode log-

134   normal distributions (Hussein et al., 2005). Thus generated are PNSDs with a diameter range of 10 nm

135   to 1 μm.

136   The H-TDMA system developed by the Guangzhou Institute of Tropical and Marine Meteorology

137   measured the size-dependent aerosol hygroscopic growth factor (GF). The H-TDMA system mainly

138   consists of four parts. The first part is a Nafion dryer to keep the RH of sampled air below 20 % and a

139   bipolar neutralizer (soft X-ray, model 3088, TSI Inc.) to equilibrate the particle charge (Wiedensohler

140   et al., 1988). Next, the sampled air passes through the first differential mobility analyzer (DMA1;

141   model 3081L, TSI Inc.) to produce mono-dispersed particles. In this study, the diameters were set to

142   40, 80, 110, 150, and 200 nm. The sampled air then went through a Nafion humidifier (model PD-70T-

143   24ss, Perma Pure Inc., USA) used to humidify the RH of sampled air to 90 %. The last part of the H-

144   TDMA is the second DMA (same model as the DMA1) and a water-based condensation particle

145   counter (model 3787, TSI Inc.), used to measure the number size distribution of humidified particles

146   in the five selected diameters. Y. Wang et al. (2017) provide a detailed introduction to the H-TDMA

147   system.

148   Size-resolved non-refractory sub-micron aerosol chemical species, including organics (Org),

149   sulfate (SO_4^{2-}), nitrate (NO_3^-), ammonium (NH_4^+), and chloride (Cl^-), were measured by the HR-AMS.

150   The sampled air dried by diffusion silica gel dryers was drawn into the HR-AMS through a $PM_{2.5}$

151   cyclone inlet to remove coarse particles larger than 2.5 μm. The HR-AMS was calibrated with pure

152   ammonium nitrate following the procedures detailed in Jimenez et al. (2003). Sun et al. (2016b)

153   provide operational details about the HR-AMS.

154   **3.   Method**

155   **3.1.   ALWC calculation based on H-TDMA measurements**

156   The ALWC is calculated based on measurements of the aerosol GF and particle number size

157   distribution. Briefly, H-TDMA data are first used to derive the size-resolved particle GFs at various

158   RHs. Then ALWC is calculated as the increased aerosol volume due to hygroscopic growth attributed

159   to water uptake.

160   Chen et al. (2012) show how to calculate size-resolved particle GFs at different RHs. First, a three-

161   mode log-normal distribution is applied to fit the measured PNSD to produce fitting parameters for

162   each mode. The hygroscopicity parameter (κ) in any mode is assumed to be constant. The H-TDMA-

163   derived size-dependent κ can then be used to deduce the corresponding κ for the nucleation mode, the

164   Aitken mode, and the accumulation mode of PNSDs according to the following equation:

165
$$\kappa(D_P) = \frac{\sum_{i=1}^3 \kappa_i \cdot N_i(D_p)}{\sum_{i=1}^3 N_i(D_p)}, \tag{1}$$

166   where κ_i refers to the κ of the ith mode, and $N_i(D_p)$ refers to the number concentration of particles in

167   the ith mode. According to κ-Köhler theory (Petters and Kreidenweis, 2007), κ at a certain diameter

168   (D_d) can be calculated as

169
$$\kappa(D_d) = (GF^3 - 1) \cdot \left[\frac{1}{RH} \exp\left(\frac{4\sigma_{s/a} M_w}{RT \rho_w D_d GF} \right) - 1 \right], \tag{2}$$

170   where RH is the control value by the humidifier in the H-TDMA system, T is the mean room

171   temperature of the container set to 293 K, $\sigma_{s/a}$ is the surface tension of the solution/air interface assumed

172 to be the same as the surface tension coefficient between water and air (about 0.0728 N m^{-1} at 293 K),

173 M_{w} is the molecular weight of water, R is the universal gas constant, ρ_{w} is the density of water, and D_{d}

174 is the diameter of the dry particles. The GF at a given RH is defined as the ratio of the humidified

175 diameter [D_{p} (RH)] to D_{d}:

176
$$GF = D_{\mathrm{p}}(\mathrm{RH})/D_{\mathrm{d}} . \tag{3}$$

177 The known κ of each mode derives the size-resolved κ at 90 % RH using Eq. (1). Substituting the size-

178 resolved κ into Eq. (2) results in size-resolved GFs at various RHs. Finally, the volume of ALWC at

179 ambient RH is equal to the increased aerosol volume due to water uptake, i.e., ALWC can be calculated

180 as

181
$$\mathrm{ALWC}_{\mathrm{HTDMA}} = \left[\frac{1}{6}\sum_i n_i D_{\mathrm{p},i}^3 \left(GF\left(\mathrm{D}_{\mathrm{p},i}, RH\right)^3 - 1\right)\right] \cdot \rho_w , \tag{4}$$

182 where n_i refers to the particle number concentration of dry particles for the corresponding particle size

183 range in the ith mode, and $D_{\mathrm{p},i}$ refers to the particle diameter for the corresponding particle size range.

184 **3.2. ALWC simulations based on the ISORROPIA II model**

185 The thermodynamic equilibrium model ISORROPIA II developed by Fountoukis and Nenes

186 (2007) using aerosol chemical composition information from the HR-AMS can simulate ALWC

187 (ALWC$_{\mathrm{ISO}}$). However, the ISORROPIA II model only considers the contribution of inorganic species

188 (Ca^{2+}, K^+, Mg^{2+}, NH^+, Na^+, SO_4^{2-}, NO_3^-, Cl^- and H_2O) on ALWC and neglects the contribution of

189 organics. In this study, the phase state was assumed to be stable in the model calculation, and the model

190 was set up to reverse mode due to the lack of measurements of gaseous ammonia.

191 According to the model assumptions that the aerosol curvature effect in Köhler theory is ignored,

192 and the aerosol water uptake has no effect on ambient vapor pressure, the water activity (a_{w}) defined

193 as the effective mole fraction of water is equal to the ambient RH in this model (Seinfeld and Pandis,

194 2006):

195
$$a_w = RH \tag{5}$$

196   The ALWC can be calculated using the Zdanovskii–Stokes–Robinson (ZSR) mixing rule (Stokes and

197   Robinson, 1966),

198
$$\mathrm{ALWC_{ISO}} = \sum_i \frac{M_i}{m_{0i}(a_w)} \, , \tag{6}$$

199   where M_i is the mole concentration of the ith species (mol m^{-3} in air), and $m_{0i}(a_w)$ is the corresponding

200   molality of the binary solution of the ith species under the same a_w with complex solution. Finally,

201   with measured ambient RH and T values as input ALWC$_{\mathrm{ISO}}$ values under different RH and T conditions

202   can be derived.

203   **3.3.   Inferring the contribution of organics to ALWC**

204   According to the κ-Köhler theory and the ZSR mixing rule, κ can also be expressed as the sum of

205   the contributions of each aerosol component:

206
$$\kappa = \sum_i \varepsilon_i \kappa_i \, , \tag{7}$$

207   where ε_i and κ_i are the volume fraction and hygroscopicity of the ith species, respectively. Submicron

208   aerosols mainly consist of organic and inorganic species (Carbone et al., 2013; Zieger et al., 2017). As

209   mentioned in section 2.2, the HR-AMS measures the mass concentrations of organics and inorganics,

210   including SO$_4^{2-}$, NO$_3^-$, NH$_4^+$, and Cl$^-$. The volume fraction of inorganic species can be calculated based

211   on the ion-pairing scheme given by the following equations (Gysel et al., 2007):

212
$$n_{\mathrm{NH_4NO_3}} = n_{\mathrm{NO_3^-}},$$

213
$$n_{\mathrm{NH_4HSO_4}} = \min\left(2n_{\mathrm{SO_4^{2-}}} - n_{\mathrm{NH_4^+}} + n_{\mathrm{NO_3^-}}, n_{\mathrm{NH_4^+}} - n_{\mathrm{NO_3^-}}\right),$$

214
$$n_{\mathrm{(NH_4)_2SO_4}} = \max\left(n_{\mathrm{NH_4^+}} - n_{\mathrm{NO_3^-}} - n_{\mathrm{SO_4^{2-}}}, 0\right),$$

215
$$n_{H_2SO_4} = \max\left(0, n_{\mathrm{SO_4^{2-}}} - n_{\mathrm{NH_4^+}} + n_{\mathrm{NO_3^-}}\right),$$

216
$$n_{\mathrm{HNO_3}} = 0, \tag{8}$$

217   where n represents the mole numbers, and "min" and "max" are minimum and maximum values,

218   respectively. The κ values of the inorganic species sulfuric acid, ammonium sulfate, ammonium

219   hydrogen sulfate, and ammonium nitrate are 1.19, 0.48, 0.56, and 0.58, respectively (Topping et al.,

220   2005; Petters and Kreidenweis, 2007). So the ZSR model can be used to estimate the contribution of

221   inorganic species to the κ value. The hygroscopicity parameter of organics (κ_{Org}) can be calculated

222   using the volume fraction of organics and the total κ value derived from the H-TDMA, according to

223   Eq. (7). Finally, the ALWC contributed by organic species (ALWC$_{Org}$) can be calculated as (Petters

224   and Kreidenweis, 2007)

225   $$\text{ALWC}_{Org} = \frac{m_{Org}\rho_W}{\rho_{Org}} \frac{\kappa_{Org}}{\left(\frac{1}{RH}-1\right)}, \qquad (9)$$

226   where m_{Org} is the organic mass concentration from the AMS (Xu et al., 2015), and ρ_{Org} is the density

227   of organics, taken as 1.4 g cm^{-3} (Moore et al., 2011; Lathem et al., 2013; Cerully et al., 2014).

4.   Results and discussion

4.1. Comparison of calculated and simulated ALWC

230   The trends in ALWC calculated based on the hygroscopic growth factor and PNSD

231   (ALWC$_{HTDMA}$) and simulated from ISOPPOPIA II model (ALWC$_{ISO}$) are generally consistent (Fig.

232   S1). However, the difference between ALWC$_{HTDMA}$ and ALWC$_{ISO}$ is large at low RH, especially at

233   ultra-low RH (< 30 %). Figure 1a shows that ALWC$_{HTDMA}$ and ALWC$_{ISO}$ agree well and that their

234   coefficient of determination (R^2) is 0.89. The correlation is especially strong for RH over 90 %.

235   However, for RH below 60 %, ALWC$_{ISO}$ is less than ALWC$_{HTDMA}$ and even close to 0 in some cases.

236   Bian et al. (2014) and Tan et al. (2017) observed a similar phenomenon in northern and southern China.

237   There are two possible explanations for these results. H-TDMA samples were humidified to 90 % RH

238   during the field campaign, thereby leading to the neglect of the deliquescence process in the

239   ALWC$_{HTDMA}$ calculation. This may lead to overestimation of ALWC$_{HTDMA}$ for RH below the

240   deliquescence relative humidity (DRH). Second, the ISORROPIA II model ignores the effect of

241   aerosol shape and complex organic species on the DRH. Previous studies have suggested that the

242   particle spherical assumption and simplified aerosol chemical species in this model can overestimate

243   the DRH (Seinfeld and Pandis, 2006; Sjogren et al., 2007). So for RH below the simulated DRH

244   (~60 %), particles may still be dry in the ISORROPIA II model, but may have been hydrated in the

245   real atmosphere. Therefore, this model underestimates ALWC. The ambient aerosol deliquescent

246   phenomenon is rare in the North China Plain (Kuang et al., 2016). In addition, the ISORROPIA II

247   model cannot simulate water uptake by organics, which can lead to some bias between simulated and

248   calculated ALWCs. As described in section 3.3, $ALWC_{Org}$ can be inferred and used to discuss

249   differences between $ALWC_{ISO}$ and $ALWC_{HTDMA}$. Figure 1b shows that adding $ALWC_{Org}$ to $ALWC_{ISO}$

250   leads to a stronger correlation with $ALWC_{HTDMA}$ ($R^2 = 0.92$). The correlation improves significantly

251   for RH below 60 %. This demonstrates that (1) organic species contribute significantly to ALWC, and

252   (2) the underestimation of ALWC by the ISORROPIA II model is also related to the neglect of organic

253   species in the model.

254

4.2.   Impact of different factors on ALWC

4.2.1.   Impact of aerosol chemical species on ALWC

257   Figure 2 shows the characteristics of seven heavy pollution events selected for examination.

258   Figures 2a and 2c display the time series of WS, WD, and ambient RH. The prevailing wind during

259   the haze episodes was a weak southerly wind that was favorable for bringing in pollutants from the

260   highly populated and industrialized neighboring regions to the sampling site. This is beneficial to the

261   formation and accumulation of SA (T. Wang et al., 2010; Y. Wang et al., 2017). However, the prevailing

262   winds during the clean events were strong northerly winds that always carried in a clean air mass,

263   resulting in pollutants being quickly removed (Figure 2c). Note that the PM_1 mass concentration

264   decreases somewhat in the evening during haze episodes, following the short-term change of WD from

265   southerly to northerly. This is related to mountain-valley breezes in Beijing (Wehner et al., 2008; Gao

266   et al., 2011; Y. Wang et al., 2017). These results demonstrate that heavy haze episodes have a strong

267   correlation with local wind direction in Beijing.

268   Figures 2a and 2d show the time series of ambient RH and mass concentrations of aerosol chemical

269   species in PM$_1$. These figures suggest that the increase in inorganic and organic aerosols is

270   synchronous with the increase in ambient RH during the heavy pollution periods (P1-P7). This is likely

271   because of a positive feedback mechanism driven by Henry's law and thermodynamic equilibrium (Z.

272   Wu et al., 2018). Figure 2b also shows that ALWC continuously increases during the pollution

273   accumulation period. On average, ALWC increases from 8 to 89 μg m^{-3} as ambient RH increases from

274   15 to 80 %, and the inorganic and organic aerosol mass concentrations increase from 15 to 120 μg m^{-3}

275   and from 12 to 78 μg m^{-3}, respectively. These results imply that the increase in ambient RH and

276   aerosol mass concentration are all important for the increase in ALWC.

277   Equation (4) also suggests that the absolute value of ALWC is dependent on the value of ambient

278   RH and aerosol chemical composition (i.e., the GF value). To further investigate the impact of

279   chemical composition on ALWC, the impact of RH on ALWC should be accounted for. Previous

280   studies suggest there is an exponential relationship between ALWC and RH (e.g., Z. Wu et al., 2018).

281   Here, we define the relative ALWC as the ratio of ALWC$_{HTDMA}$ and the function of ambient RH (e^{bRH}).

282   Figure 3a shows the relationship between relative ALWC and primary aerosols (PA) or SA mass

283   concentrations. PA consists of primary organic aerosols (POA) and black carbon (BC), and SA consists

284   of SOA, sulfate, and nitrate. The relative ALWC is highly correlated with SA mass concentrations (R^2

285   = 0.94) but poorly correlated with PA mass concentrations (R^2 = 0.69). High relative ALWCs

286   coincident with high SA mass concentrations suggest that SA plays a key role in the increase in ALWC.

287   This is likely because SA is mainly generated from photochemical reactions in the daytime or reactions

288   at night, making SA highly aged with a hygroscopicity stronger than that of PA (Ervens et al., 2011;

289   Sareen et al., 2017). SA can, therefore, absorb more water vapor than PA in the atmosphere. The

290   enhanced aerosol liquid water induced by SA is further favorable for the formation of SA by speeding

291   up the atmospheric chemical reaction rate and serving as the medium for gas-particle heterogeneous

292   reactions (G. Wang et al., 2016; Cheng et al., 2016). This further increases the bulk aerosol

293   hygroscopicity. This is also the reason why inferred κ based on the ZSR model continuously increases

294   during haze episodes (Figure 2c).

295   Secondary aerosols are mainly composed of nitrate, sulfate, and SOA. To determine which species

296   is the driver for ALWC in Beijing, Figure 3b shows the correlation analysis between relative ALWC

297   and the mass concentrations of different aerosol chemical species. Relative ALWC and all SIA agree

298   well [R^2 equal to 0.66 (sulfate) and 0.56 (nitrate)]. It has been reported that ALWC is driven by

299   inorganic salts with both nitrate and sulfate playing key roles in determining ALWC (Z. Wu et al.,

300   2018). ALWC also agrees well with SOA ($R^2 = 0.60$) in our study. This is unexpected because the

301   hygroscopicity of SOA is relatively lower than that of nitrate and sulfate. Some studies have also

302   suggested that the water uptake of aged organics accounts for only a few percent of the total aerosol

303   water uptake (e.g., Gysel et al., 2007; Engelhart et al., 2011). In our study, the contribution of $ALWC_{Org}$

304   to total ALWC is significant, accounting for 30 % ± 22 %. Studies of ALWC in Beijing, therefore,

305   cannot neglect $ALWC_{Org}$. This is different from the studies in other regions such as in the Po Valley in

306   Italy (Hodas et al., 2014) and the eastern U.S. (Carlton et al., 2013) where the ALWC was found to be

307   only driven by nitrate and sulfate respectively.

308   An interesting phenomenon is frequently observed at the initial stage of heavy haze episodes (e.g.,

309   P4, P5, P6, and P7). $ALWC_{ISO}$ is almost close to 0, but both $ALWC_{HTDMA}$ and $ALWC_{Org}$ are always

310   larger than 0, and the organic aerosol mass fraction is high at this stage. These observations reveal that

311   at the initial stage of heavy haze episodes, the ALWC is mostly contributed by organic species.

312   Meanwhile, κ is not very low and increases markedly as the PM_1 mass concentration increases, which

313   is unexpected because of the lower hygroscopicity of organic aerosols compared to SIA. Therefore,

314   some highly hygroscopic substance (i.e., SA) must be generated through multiphase chemical reaction

315   at this stage. We propose that the liquid water contributed by organic species provides a reactor for the

316   transformation of gaseous precursors to SA at the initial stages of heavy haze episodes, increasing the

317   uptake of more liquid water by more SA and further accelerating the formation of heavy haze. Section

318   4.3 provides a case study to demonstrate this.

319   **4.2.2. Impact of PNSD on ALWC**

320   In addition to aerosol chemical composition, ALWC also depends on PNSD (Bian et al., 2014).

321   As described in section 3.1, the nucleation mode (< 30 nm), the Aitken mode (30–110 nm), and the

322   accumulation mode (110 nm to1 μm) (Whitby, 1978; Birmili et al., 2001) are considered in this study.

323   Particles with diameters greater than 1 μm are not considered because most of these large particles are

324   composed of hydrophobic species (e.g., dust or mineral substances) that contribute little to ALWC

325   (Hussein et al., 2004; S. Liu et al., 2008; Bian et al., 2014; Tan et al., 2017).

326   Figure S2 in the supplement shows that the contributions of nucleation mode, Aitken mode, and

327   accumulation mode particles to ALWC are < 1.0 %, 18.0 %, and 82.0 %, respectively. Figure 4 shows

328   the correlations between $ALWC_{HTDMA}$ and the volume concentrations of different mode particles, and

329   the average contribution of different mode particles to $ALWC_{HTDMA}$ (f_{ALWC}) under five different RH

330   conditions. The R^2 and f_{ALWC} of the nucleation mode particles (left column in Figure 4) are all less than

331   0.1 and 1 %, respectively, under all RH conditions. This is likely because the volume concentration of

332   nucleation mode particles is very low, and most of these small particles are composed of hydrophobic

333   chemical species such as BC and POA. Similarly, the number concentration of Aitken mode particles

334   also shows weak correlations with $ALWC_{HTDMA}$ ($R^2 < 0.2$) under RH < 90 % conditions, but their

335   correlation ($R^2 = 0.25$) is enhanced significantly under RH > 90 % conditions (middle column of Figure

336   4). This is because there are more aged particles in the Aitken mode which can absorb much more

337   water when the ambient RH is higher than 90 %. However, the contribution of the Aitken mode to

338   ALWC ranges from 14 % to 21 % and decreases as RH increases. $ALWC_{HTDMA}$ is strongly correlated

339   to the volume concentration of accumulation mode particles, with R^2 and f_{ALWC} greater than 0.6 and

340   75 %, respectively, under all RH conditions (right column of Figure 4). Figure 4 also shows that ALWC

341   increases slightly as the volume concentration of accumulation mode particles increases under RH <

342   70 % conditions (slope < 0.001), but increases strongly under higher RH conditions, especially under

343   RH > 90 % conditions (slope = 0.0041). This is likely because there are more accumulation mode SA

344   formed due to multiphase chemical reactions under high ambient RH conditions. Swietlicki et al.

345   (1999) have suggested that the contribution of accumulation mode particles to ALWC is largest for all-

346   mode particles.

347   In summary, the contribution of nucleation mode particles to ALWC is very low. The contribution

348   of Aitken mode particles is much higher than nucleation mode particles and decreases with increasing

349   ambient RH. The contribution of accumulation mode particles to ALWC is largest under all RH

350   conditions and increases with increasing ambient RH, thus playing a key role in determining ALWC.

351   **4.2.3.   Impact of RH on ALWC**

352   As discussed in 4.2.1, the absolute value of ALWC has an exponential relationship with ambient

353   RH. Figure 5 shows the relationship between ALWC and RH for different PM_1 mass concentration

354   ranges. ALWC increases slowly as RH increases under lower ambient RH conditions then sharply

355   increases when RH exceeds a critical RH value. This critical RH value is different for different PM_1

356   mass concentrations. This is because the low RH conditions cannot provide enough water for aerosol

357   particles, even though the PNSD is dominated by accumulation mode particles with higher

358   hygroscopicity (Tan et al., 2016). This demonstrates the important influence of RH on ALWC. The

359   lower critical RH value for higher PM_1 mass concentrations (~80 %) suggests that ALWC is easily

360   formed under heavily polluted conditions. This is likely because there are more SA and accumulation

361   mode particles during pollution periods (Sun et al., 2016a; Y. Wang et al., 2017).

362   Figure 6a shows the diurnal variations of $ALWC_{HTDMA}$ and ambient RH during the sampling

363   period. The extreme $ALWC_{HTDMA}$ values appear at night and during the day respectively, likely related

364   to the diurnal variations of ambient RH. The elevated ambient RH at night not only increases ALWC

365   through water uptake of particles directly, but also facilitates the formation of hydrophilic particulate

366   nitrate through the speeding up of the uptake coefficient of N_2O_5 (Thornton et al., 2003; Bertram et

367   al., 2009). This can further enhance ALWC. However, although the diurnal variations of $ALWC_{HTDMA}$

368   and ambient RH are similar, the peak and nadir of $ALWC_{HTDMA}$ (0300 LT and 1100 LT, respectively)

369   appear three hours earlier than the peak and nadir of ambient RH (0600 LT and 1400 LT, respectively).

370   This time difference is likely related to changes in PNSD. The diurnal variation of PNSD (Figure 6b)

371   shows that the number concentrations of Aitken and accumulation mode particles begin to decrease

372   quickly at 0300 LT. ALWC also begins to decrease, although the ambient RH increases slightly at that

373   time. In the morning, ALWC decreases sharply following the ambient RH and PNSD changes due to

374   the lifting planetary boundary layer height. ALWC decreases to its minimum value at ~1100 LT then

375   begins to increase quickly. However, ambient RH still decreases at that time and reaches its minimum

376   value at ~1400 LT. The increase in ALWC is likely associated with changes in aerosol chemical species

377   and PNSD. Figure 6b and 6c show that there are many newly formed Aitken and accumulation mode

378   particles and that the fraction of SA increases at noon, likely because of strong photochemical

379   reactions. Y. Wang et al. (2017, 2018) have suggested that daytime photochemical reactions are

380   efficient enough to enhance aerosol hygroscopicity and change the aerosol mixing state from external

381   to internal in North China through the formation of hydrophilic chemical species. All this suggests that

382   ambient RH is not the only determining factor for ALWC. PNSD and aerosol chemical composition

383   are also important for ALWC.

384   **4.3.   A case study of the impact of $ALWC_{Org}$ on SA formation**

385   As discussed in section 4.2.1, a hypothesis is proposed that $ALWC_{Org}$ maybe provide a reactor for

386   the formation of secondary species. To verify this hypothesis, the P4 case shown in Figure2 is selected

387   to further analyze the influence of $ALWC_{Org}$ on the formation of secondary aerosols (Figure 7). Figure

388   7a shows the time series of $ALWC_{HTDMA}$, $ALWC_{ISO}$, and $ALWC_{Org}$ during this case. On 27 November

389   2017, $ALWC_{ISO}$ was close to 0 all day long because of the low ambient RH, but both $ALWC_{HTDMA}$ and

390   $ALWC_{Org}$ were always larger than 0, increasing with increasing PM_1 mass concentration (Figure 7a).

391   Figure 7a also shows that the fraction of $ALWC_{Org}$ in $ALWC_{HTDMA}$ was high at the initial stage of this

392   pollution case, but this fraction decreased as haze increased. This case was further divided into three

393   periods (Figure 7b). Organics were the most abundant chemical species during the first period (64 %),

394   which explains the high fraction of $ALWC_{Org}$ in $ALWC_{HTDMA}$ at the initial stage of this haze case. The

395   pie charts in Figure 7b also show that both SOA and SIA (sulfate, nitrate, and ammonium) increases

396   from the first to third periods but POA decreases, likely related to multiphase reactions (i.e., aqueous-

397   phase reactions) due to the enhanced ALWC. Time series of f_{44} and the fraction of sulfate in total sulfur

398    $(F_{SO4^{2-}})$ are also shown to further illustrate the influence of aqueous-phase reactions on aerosol

399   chemical species. The m/z 44 signal intensity f_{44} (mostly contributed by the CO_2^+ ion) measured by the

400   AMS can be used as an indicator of the oxidation level in organic species (Mei et al., 2013). The sulfur

401   oxidation ratio $F_{SO4^{2-}}$ (Sun et al., 2006) is defined as

$$F_{SO_4^{2-}} = \frac{n[SO_4^{2-}]}{n[SO_4^{2-}]+n[SO_2]} , \qquad (10)$$

403   where $n[SO_4^{2-}]$ and $n[SO_2]$ refer to the molar concentrations of SO_4^{2-} and SO_2, respectively. Figure 7b

404   suggests that f_{44} and $F_{SO4^{2-}}$ both increase gradually with increasing $ALWC_{HTDMA}$ and PM_1 mass

405   concentration from 27 November to 30 November 2017. This is likely because the increase in ALWC

406   is beneficial to the oxidation of organics and the transformation of SO_2 to SO_4^{2-}, implying the

407   importance of aqueous-phase chemical reaction on haze formation in Beijing. The production of

408   secondary organic and inorganic species can further enhance aerosol hygroscopicity, increasing ALWC

409   in the atmosphere. This positive feedback is the reason behind the rapid formation of heavy haze events

410   in Beijing (G. Wang et al., 2016). A rapid increase in f_{44} and $F_{SO4^{2-}}$ was seen during the first period at

411   night on 27 November (shown by green and red arrows in Fig. 7) when organics contributed the most

412   to ALWC. This suggests that ALWC contributed by organics may have played an important role in the

413   formation of secondary species at the initial stage of the pollution event.

414

5. Conclusions

In this study, the aerosol liquid water content (ALWC) was calculated using the size-resolved aerosol hygroscopic growth factor and the particle number size distribution (PNSD) measured at a Beijing urban site during the APHH winter campaign (8 November to 15 December 2017). Also done were simulations using the ISORROPIA II model with measured aerosol chemical composition data as input data. During the sampling period, seven heavy haze episodes were selected to investigate the influence of different factors (PNSD, ambient RH, and aerosol chemical composition) on ALWC.

The calculated and simulated ALWC ($ALWC_{HTDMA}$ and $ALWC_{ISO}$) agree well (correlation of determination R^2 equal to 0.89). However, $ALWC_{ISO}$ is much lower than $ALWC_{HTDMA}$ for RH below 60 %, even approaching zero many times. This deviation is in part attributed to the neglect of the contribution of organics to ALWC ($ALWC_{Org}$) in the ISORROPIA II model, contradicting with previous studies ignoring this contribution. The aerosol hygroscopicity of organics was also derived in this study for use in calculating $ALWC_{Org}$. The sum of $ALWC_{ISO}$ and $ALWC_{Org}$ has a higher correlation ($R^2 = 0.92$) with the calculated ALWC (i.e., $ALWC_{HTDMA}$), especially for RH below 60 %. This implies that organic aerosols are also an important contributor to ALWC.

PNSD, ambient RH, and aerosol chemical composition are all found to affect ALWC significantly. Nucleation mode and Aitken mode particles have little influence on ALWC. Accumulation mode particles play a key role in determining ALWC and dominate among all aerosol modes. ALWC is highly related to the relative humidity (RH) when RH exceeds a critical RH value that is different for different PM_1 mass concentrations. ALWC varies diurnally with its extreme values appearing at night and during the day respectively. The diurnal variation of ambient RH explains this. However, there is a three-hour difference between when the extreme ALWC and RH values occur, caused by the diurnal variations in PNSD and aerosol chemical composition.

On average, $ALWC_{Org}$ accounts for ~30 % ± 22 % of the total aerosol liquid water during the sampling period. This shows the significant contribution of organic species to ALWC. Our results

440   suggest that ALWC is not only driven by inorganic salts but also driven by organics in Beijing. This is

441   different from the results obtained in the Po Valley in Italy (Hodas et al., 2014) and the eastern U.S.

442   (Carlton et al., 2013) where the ALWC is driven by nitrate and sulfate respectively. Finally, one case

443   study was used to study the importance of $ALWC_{Org}$ on multiphase chemical reactions. $ALWC_{Org}$ was

444   found to play an important role in the formation of secondary aerosols by speeding up aqueous-phase

445   reactions at the initial stage of heavy haze. Our study is important for investigating the contribution of

446   organics to ALWC and its importance on haze formation in Beijing.

447

448   *Data availability.* Data used in the study are available from the first author upon request

449   (201631490012@mali.bnu.edu.cn).

450

451   *Author contributions.* ZL and YW designed the experiment; YW, XJ, and WX carried it out and

452   analyzed the data; other co-authors participated in science discussions and suggested additional

453   analyses. XJ and YW prepared the paper with contributions from all co-authors.

454

455   *Competing interests.* The authors declare no competing interests.

456

457   *Acknowledgements.* This work was funded by the National Key R&D Program of China (grant no.

458   2017YFC1501702), National Natural Science Foundation of China (NSFC) research projects (grant

459   nos. 91544217, 41575143, 41675141, 41705125), and the National Basic Research Program of China

460   "973" (grant no. 2013CB955801). We thank all participants of the field campaign for their tireless

461   work and cooperation.

462

463   **References**
464

465   Abbatt, J. P. D., Lee, A. K. Y., Thornton, J. A.: Quantifying Trace Gas Uptake to Tropospheric Aerosol:

466   Recent Advances and Remaining Challenges, Chem. Soc. Rev., 41(19), 6555−6581,
467   https://doi.org/10.1039/c2cs35052a, 2012.

468 Adams, P. J., Seinfeld, J. H.: General circulation model assessment of direct radiative forcing by the
469   sulfate-nitrate−ammonium−water inorganic aerosol system, J. Geophys. Res.-Atmos., 106,
470   1097−1111, https://doi.org/ 10.1029/2000JD900512, 2001.

471 Ansari, A.S., Pandis, S.N.: Prediction of multicomponent inorganic atmospheric aerosol behavior,
472   Atmos. Environ., 33 (5), 745–757, https://doi.org/10.1016/S1352-2310(98)00221-0, 1999.

473 Arellanes, C., Paulson, S. E., Fine, P. M., and Sioutas, C.: Exceeding of Henry's Law by Hydrogen
474   Peroxide Associated with Urban Aerosols, Environ. Sci. Technol., 40, 4859–4866,
475   https://doi.org/10.1021/es0513786, 2006.

476 Bertram, T. H., Thornton, J. A.: Toward a general parameterization of N_2O_5 reactivity on aqueous
477   particles: the competing effects of particle liquid water, nitrate and chloride, Atmos. Chem. Phys., 9
478   (21), 8351−8363, https://doi.org/10.5194/acp-9-8351-2009, 2009.

479 Bian, Y.X., Zhao, C.S., Ma, N., Chen, J., Xu, W.Y.: A study of aerosol liquid water content based on
480   hygroscopicity measurements at high relative humidity in the North China Plain, Atmos. Chem.
481   Phys., 14 (12), 6417–6426, https://doi.org/10.5194/acp-14-6417-2014, 2014.

482 Birmili, W., Wiedensohler, A., Heintzenberg, J., and Lehmann, K.: Atmospheric particle number size
483   distribution in central Europe: Statistical relations to air masses and meteorology, J. Geophys. Res.-
484   Atmos., 106, 32005–32018, https://doi.org/10.1029/2000JD000220, 2001.

485 Blando, J. D., Turpin, B. J.: Secondary organic aerosol formation in cloud and fog droplets: a literature
486   evaluation of plausibility, Atmos. Environ., 34, 1623−1632, https://doi.org/10.1016/S1352-
487   2310(99)00392-1, 2001.

488 Carbone, S., Saarikoski, S., Frey, A., Reyes, F., Reyes, P., Castillo, M., Gramsch, E., Oyola, P., Jayne,
489   J., Worsnop, DR., and Hillamo, R.: Chemical characterization of submicron aerosol particles in
490   Santiago de Chile, Aerosol Air Qual. Res., 13(2), 462-473,
491   https://doi.org/10.4209/aaqr.2012.10.0261, 2013.

492 Carlton, A. G., Turpin, B. J.: Particle partitioning potential of organic compounds is highest in the
493   Eastern US and driven by anthropogenic water, Atmos. Chem. Phys., 13 (20), 10203−10214,
494   https://doi.org/10.5194/acp-13-10203-2013, 2013.

495 Cerully, K. M., Bougiatioti, A., Hite Jr., J. R., Guo, H., Xu, L., Ng, N. L., Weber, R., and Nenes, A.:
496   On the link between hygroscopicity, volatility, and oxidation state of ambient and water-soluble
497   aerosol in the Southeastern United States, Atmos. Chem. Phys., 14, 30835–30877,
498   https://doi.org/10.5194/acpd-14-30835- 2014, 2014.

499 Chen, J., Zhao, C. S., Ma, N., Liu, P. F., Göbel, T., Hallbauer, E., Deng, Z. Z., Ran, L., Xu, W. Y.,

Liang, Z., Liu, H. J., Yan, P., Zhou, X. J., and Wiedensohler, A.: A parameterization of low visibilities for hazy days in the North China Plain, Atmos. Chem. Phys., 12, 4935–4950, https://doi.org/10.5194/acp-12-4935-2012, 2012.

Cheng, Y., Zheng, G., Wei, C., Mu, Q., Zheng, B., Wang, Z., Gao, M., Zhang, Q., He, K., Carmichael, G., Pöschl, U., Su, H.: Reactive nitrogen chemistry in aerosol water as a source of sulfate during haze events in China, Sci. Adv., 2 (12), e1601530, https://doi.org/10.1126/sciadv.1601530, 2016.

Dougle, P. G., Vlasenko, A. L., Veefkind, J. P., and Brink, H. M. T.: Humidity dependence of the light scattering by mixtures of ammonium nitrate, ammonium sulfate and soot, J. Aerosol. Sci., 27, 513–514, https://doi.org/10.1016/0021-8502(96)00329-1, 1996.

Engelhart, G.J., Hildebrandt, L., Kostenidou, E., Mihalopoulos, N., Donahue, N.M., Pandis, S.N.: Water content of aged aerosol, Atmos. Chem. Phys., 11, 911–920, https://doi.org/10.5194/acp-11-911-2011, 2011.

Ervens, B., Turpin, B. J., Weber, R. J.: Secondary organic aerosol formation in cloud droplets and aqueous particles (aqSOA): a review of laboratory, field and model studies, Atmos. Chem. Phys., 11 (21), 11069−11102, https://doi.org/10.5194/acp-11-11069-2011, 2011.

Fountoukis, C. and Nenes, A.: ISORROPIA II: a computationally efficient thermodynamic equilibrium model for K^+– Ca^{2+}–Mg^{2+}–$NH4^+$–Na^+–$SONO$ –Cl^-–H_2O aerosols, Atmos. Chem. Phys., 7, 4639–4659, https://doi.org/10.5194/acp-7-4639-2007, 2007.

Gao, Y., Liu, X., Zhao, C., and Zhang, M.: Emission controls versus meteorological conditions in determining aerosol concentra- tions in Beijing during the 2008 Olympic Games, Atmos. Chem. Phys., 11, 12437–12451, https://doi.org/10.5194/acp-11-12437-2011, 2011.

Gysel, M., Grosier, J., Topping, D.O., Whitehead, J.D., Bower, J.N., Cubison, M.J., Williams, P.I., Flynn, M.J., McFiggans, G.B., Coe, H.: Closure study between chemical composition and hygroscopic growth of aerosol particles during TORCH2, Atmos. Chem. Phys., 7 (24), 6131–6144, https://doi.org/10.5194/acp-7-6131-2007, 2007.

Hennigan, C. J., Bergin, M. H., Dibb, J. E., Weber, R. J.: Enhanced secondary organic aerosol formation due to water uptake by fine particles, Geophys. Res. Lett., 35(18), No. L18801, https://doi.org/10.1029/2008GL035046, 2008.

Hodas, N., Sullivan, A. P., Skog, K., Keutsch, F. N., Collett, J. L., Decesari, S., Facchini, M. C., Carlton, A. G., Laaksonen, A., Turpin, B. J.: Aerosol Liquid Water Driven by Anthropogenic Nitrate: Implications for Lifetimes of Water-Soluble Organic Gases and Potential for Secondary Organic Aerosol Formation, Environ. Sci. Technol., 48 (19), 11127−11136 https://doi.org/10.1021/es5025096, 2014.

533 Huang, R., Zhang, Y., Bozzetti, C., Ho, K., Cao, J., Han, Y., Daellenbach, K. R., Slowik, J. G., Platt,
534   S. M., Canonaco, F.: High secondary aerosol contribution to particulate pollution during haze events
535   in China, Nature., 514 (7521), 218, https://doi.org/10.1038/nature13774, 2014,.

536 Hussein, T., Puustinen, A., Aalto, P. P., Mäkelä, J. M., Hämeri, K., and Kulmala, M.: Urban aerosol
537   number size distributions, Atmos, Chem. Phys., 4, 391–411, https://doi.org/10.5194/acp-4-391-
538   2004, 2004.

539 Hussein, T., Dal Maso, M., Petäjä, T., Koponen, I. K., Paatero, P., Aalto, P. P., Hämeri, K., and Kulmala,
540   M.: Evaluation of an automatic algorithm for fitting the particle number size distributions, Boreal
541   Environ. Res., 10, 337–355, 2005.

542 Jimenez, J. L., Jayne, J. T., Shi, Q., Kolb, C. E., Worsnop, D. R., Yourshaw, I., Morris, J. W.: Ambient
543   aerosol sampling using the aerodyne aerosol mass spectrometer, J. Geophys. Res.-Atmos., 108(D7),
544   https://doi.org/ https://doi.org/10.1029/2001JD001213, 2003.

545 Kim, Y.P., Seinfeld, J.H., Saxena, P.: Atmospheric gas-aerosol equilibrium I. Thermodynamic model,
546   Aerosol Sci. Technol., 19 (2), 157–181, https://doi.org/10.1080/02786829308959628, 1993.

547 Kitamori, Y., Mochida, M., Kawamura, K.: Assessment of the aerosol water content in urban
548   atmospheric particles by the hygroscopic growth measurements in Sapporo, Japan. Atmos. Environ.,
549   43 (21), 3416–3423, https://doi.org/10.1016/j.atmosenv.2009.03.037, 2009.

550 Kuang Y., Zhao C.S., Ma N., Liu H.J., Bian Y.X., Tao J.C. and Hu M.: Deliquescent phenomena of
551   ambient aerosols on the North China Plain, Geophys Res Lett, 43, 8744-8750,
552   https://doi.org/10.1002/2016GL070273, 2016.

553 Kuang, Y., Zhao, C. S., Zhao, G., Tao, J. C., Xu, W., Ma, N., and Bian, Y. X.: A novel method for
554   calculating ambient aerosol liquid water content based on measurements of a humidified
555   nephelometer system, Atmospheric Measurement Techniques, 11(5), 2967-2982,
556   https://doi.org/10.5194/amt-11-2967-2018, 2018.

557 Lathem, T. L., Beyersdorf, A. J., Thornhill, K. L., Winstead, E. L., Cubison, M. J., Hecobian, A.,
558   Jimenez, J. L., Weber, R. J., Anderson, B. E., and Nenes, A.: Analysis of CCN activity of Arctic
559   aerosol and Canadian biomass burning during summer 2008, Atmos. Chem. Phys., 13, 2735–2756,
560   https://doi.org/10.5194/acp-13-2735- 2013, 2013.

561 Liao, H., Seinfeld, J. H.: Global impacts of gas-phase chemistry aerosol interactions on direct radiative
562   forcing by anthropogenic aerosols and ozone, J. Geophys. Res.-Atmos., 110 (D18).
563   https://doi.org/10.1029/ 2005JD005907, 2005.

564 Li, Z., Lau, W. M., Ramanathan, V., Wu, G., Ding, Y., Manoj, M. G., Liu, J., Qian, Y., Li, J., and Zhou,
565   T.: Aerosol and mon- soon climate interactions over Asia, Rev. Geophys., 54, 866–929,
566   https://doi.org/10.1002/2015RG000500, 2016.

567 Liu, S., Hu, M., Wu, Z., Wehner, B., Wiedensohler, A., and Cheng, Y.: Aerosol number size distribution
568   and new particle formation at a rural/coastal site in Pearl River Delta (PRD) of China, Atmos.
569   Environ., 42, 6275–6283, https://doi.org/10.1016/j.atmosenv.2008.01.063, 2008.

570 Mei F., Setyan A., Zhang Q. and Wang J.: CCN activity of organic aerosols observed downwind of
571   urban emissions during CARES, Atmos. Chem. Phys., 13, 12155-12169,
572   https://doi.org/10.5194/acp-13-12155-2013, 2013.

573 Moore, R. H., Bahreini, R., Brock, C. A., Froyd, K. D., Cozic, J., Holloway, J. S., Middlebrook, A. M.,
574   Murphy, D. M., and Nenes, A.: Hygroscopicity and composition of Alaskan Arctic CCN during
575   April 2008, Atmos. Chem. Phys., 11, 11807–11825, https://doi.org/10.5194/acp-11-11807-2011,
576   2011.

577 Nenes, A., Pandis, S.N., Pilinis, C.: ISORROPIA: a new thermodynamic equilibrium model for
578   multiphase multicomponent inorganic aerosols, Aquat. Geochem., 4 (1), 123–152,
579   https://doi.org/10.1023/A:1009604003981, 1998.

580 Nguyen, T. K. V., Zhang, Q., Jimenez, J. L., Pike, M., Carlton, A. G.: Liquid Water: Ubiquitous
581   Contributor to Aerosol Mass, Environ. Sci. Technol. Lett., 3 (7), 257−263,
582   https://doi.org/10.1021/acs.estlett.6b00167, 2016.

583 Petters, M. D. and Kreidenweis, S. M.: A single parameter representation of hygroscopic growth and
584   cloud condensation nucleus activity, Atmos. Chem. Phys., 7, 1961–1971,
585   https://doi.org/10.5194/acp-7- 1961-2007, 2007.

586 Sareen, N., Waxman, E. M., Turpin, B. J., Volkamer, R., Carlton, A. G.: Potential of Aerosol Liquid
587   Water to Facilitate Organic Aerosol Formation: Assessing Knowledge Gaps about Precursors and
588   Partitioning, Environ. Sci. Technol., 51 (6), 3327−3335, https://doi.org/10.1021/acs.est.6b04540,
589   2017.

590 Seinfeld, H. J., Pandis, N. S.: Atmospheric Chemistry and Physics: From Air Pollution to Climate
591   Change, Taylor & Francis Group, https://doi.org/10.1080/00139157.1999.10544295, 2006.

592 Sjogren, S., Gysel, M., Weingartner, E., Baltensperger, U., Cubison, M. J., Coe, H., Zardini, A. A.,
593   Marcolli, C., Krieger, U. K., and Peter, T.: Hygroscopic growth and water uptake kinetics of two-
594   phase aerosol particles consisting of ammonium sulfate, adipic and humic acid mixtures, J. Aerosol.
595   Sci., 38, 157–171, https://doi.org/10.1016/j.jaerosci.2006.11.005, 2007.

596 Song, S., Gao, M., Xu, W., et al.: Possible heterogeneous chemistry of hydroxyl-methane-sulfonate
597   (HMS) in northern China winter haze, Atmos. Chem. Phys., 19(2): 1357-1371,
598   https://doi.org/10.5194/acp-19-1357-2019, 2019.

599 Stanier, C.O., Khlystov, A.Y., Chan, W.R., Mandiro, M., Pandis, S.N.: A method for the in situ
600   measurement of fine aerosol water content of ambient aerosols: The Dry Ambient Aerosol Size

601   Spectrometer   (DAASS),   Aerosol   Sci.   Technol.,   38   (1),   215–228,
602   https://doi.org/10.1080/02786820390229525, 2004.

603   Stokes, R. H. and Robinson, R. A.: Interactions in aqueous nonelectrolyte solutions. I. Solute-solvent
604   equilibria, J. Phys. Chem., 70, 2126–2131, https://doi.org/10.1021/j100879a010, 1966.

605   Sun, Y., Zhuang, G., Tang, A., Wang, Y., An, Z.: Chemical characteristics of $PM_{2.5}$ and PM_{10} in haze-
606   fog episodes in Beijing, Environ. Sci. Technol., 40, 3148-3155, https://doi.org/10.1021/es051533g,
607   2006.

608   Sun, Y., Z. F. Wang, P. Q. Fu, T. Yang, Q. Jiang, H. B. Dong, J. Li, and J. J. Jia.: Aerosol composition,
609   sources and processes during wintertime in Beijing, China, Atmos. Chem. Phys., 13(9), 4577–4592,
610   https://doi.org/10.5194/acp-13-4577-2013, 2013.

611   Sun Y., Chen C., Zhang Y., Xu W., Zhou L., Cheng X., Zheng H., Ji D., Jie L. and Xiao T.: Rapid
612   formation and evolution of an extreme haze episode in Northern China during winter 2015, Sci.
613   Rep., 6(1):27151, https://doi.org/10.1038/srep27151, 2016a.

614   Sun, Y., Wang, Z., Wild, O., Xu, W., Chen, C., Fu, P., Du, W., Zhou, L., Zhang, Q., and Han, T.: "APEC
615   Blue": Secondary Aerosol Reductions from Emission Controls in Beijing, Sci. Rep., 6, 20668,
616   https://doi.org/10.1038/srep20668, 2016b.

617   Surratt, J. D., Kroll, J. H., Kleindienst, T. E., Edney, E. O., Claeys, M., Sorooshian, A., Ng, N. L.,
618   Offenberg, J. H., Lewandowski, M., Jaoui, M., Flagan, R. C., Seinfeld, J. H.: Evidence for
619   organosulfates   in   secondary   organic   aerosol,   Environ.   Sci.   Technol.,   41,   517−527,
620   https://doi.org/10.1021/es062081q, 2007.

621   Swietlicki, E., Zhou, J., Berg, O. H., Martinsson, B. G., Frank, G., Cederfelt, S. I., Dusek, U., Berner,
622   A., Birmili, W., Wiedensohler, A., Yuskiewicz, B., and Bower, K. N.: A closure study of sub-
623   micrometer   aerosol   particle   hygroscopic   behaviour,   Atmos.   Res.,   50,   205–240,
624   https://doi.org/10.1016/S0169-8095(98)00105-7, 1999.

625   Tan, H., Cai, M., Fan, Q., Liu, L., Li, F., & Chan, P. W., et al.: An analysis of aerosol liquid water
626   content and related impact factors in pearl river delta, Science of The Total Environment, 579, 1822-
627   1830, https://doi.org/10.1016/j.scitotenv.2016.11.167, 2017.

628   Tao, W. K., Chen, J. P., Li, Z., Wang, C., and Zhang, C.: Impact of Aerosols on Convective Clouds and
629   Precipitation, Rev. Geo. phys., 50, 1–62, https://doi.org/10.1029/2011RG000369, 2012.

630   Thornton, J. A., Braban, C. F., Abbatt, J. P. D.: N_2O_5 hydrolysis on sub-micron organic aerosols: the
631   effect of relative humidity, particle phase, and particle size. Atmos. Chem. Phys., 5 (20), 4593−4603,
632   https://doi.org/10.1039/b307498f, 2003.

633   Topping D O, Mcfiggans G B, Coe H.: A curved multi-component aerosol hygroscopicity model

634   framework: Part 1 – Inorganic compounds, Atmos. Chem. Phys., 5(5): 1205-1222,
635   https://doi.org/10.5194/acp-5-1205-2005, 2005.

636   Wahner, A., Mentel, T. F., Sohn, M., Stier, J.: Heterogeneous reaction of N_2O_5 on sodium nitrate
637   aerosol, J. Geophys. Res. Atmos, 103 (D23), 31103−31112, https://doi.org/10.1029/1998JD100022,
638   1998.

639   Wang, G., Zhang, R., Gomez, M. E., Yang, L., Levy Zamora, M., Hu, M., Lin, Y., Peng, J., Guo, S.,
640   Meng, J., Li, J., Cheng, C., Hu, T., Ren, Y., Wang, Y., Gao, J., Cao, J., An, Z., Zhou, W., Li, G.,
641   Wang, J., Tian, P., MarreroOrtiz, W., Secrest, J., Du, Z., Zheng, J., Shang, D., Zeng, L., Shao, M.,
642   Wang, W., Huang, Y., Wang, Y., Zhu, Y., Li, Y., Hu, J., Pan, B., Cai, L., Cheng, Y., Ji, Y., Zhang, F.,
643   Rosenfeld, D., Liss, P. S., Duce, R. A., Kolb, C. E., Molina, M. J.: Persistent sulfate formation from
644   London Fog to Chinese haze, Proc. Natl. Acad. Sci. U. S. A., 113 (48), 13630−13635,
645   https://doi.org/10.1073/pnas.1616540113, 2016.

646   Wang, H., Lu, K., Chen, X., Zhu, Q., Chen, Q., Guo, S., Jiang, M., Li, X., Shang, D., Tan, Z., Wu, Y.,
647   Wu, Z., Zou, Q., Zheng, Y., Zeng, L., Zhu, T., Hu, M., Zhang, Y.: High N_2O_5 Concentrations
648   Observed in Urban Beijing: Implications of a Large Nitrate Formation Pathway, Environ. Sci.
649   Technol. Lett., 4 (10), 416−420, https://doi.org/10.1021/acs.estlett.7b00341, 2017.

650   Wang, T., Nie, W., Gao, J., Xue, L. K., Gao, X. M., Wang, X. F., Qiu, J., Poon, C. N., Meinardi, S.,
651   Blake, D., Wang, S. L., Ding, A. J., Chai, F. H., Zhang, Q. Z., and Wang, W. X.: Air quality during
652   the 2008 Beijing Olympics: secondary pollutants and regional impact, Atmos. Chem. Phys., 10,
653   7603–7615, https://doi.org/10.5194/acp-10-7603-2010, 2010.

654   Wang, Y., Zhang, Q., Jiang, J., Zhou, W., Wang, B., He, K., Duan, F., Zhang, Q., Philip, S., and Xie,
655   Y.: Enhanced sulfate formation during China's severe winter haze episode in January 2013 missing
656   from   current   models,   J.   Geophys.   Res.-Atmos.,   119,   10425–   10440,
657   https://doi.org/10.1002/2013JD021426, 2014.

658   Wang Y., Zhang F., Li Z., Tan H., Xu H., Ren J., Zhao J., Du W. and Sun Y.: Enhanced hydrophobicity
659   and volatility of submicron aerosols under severe emission control conditions in Beijing, Atmos
660   Chem Phys, 17, 5239-5251, https://doi.org/10.5194/acp-17-5239-2017, 2017.

661   Wang Y., Li Z., Zhang Y., Du W., Zhang F., Tan H., Xu H., Fan T., Jin X., Fan X., Dong Z., Wang Q.
662   and Sun Y.: Characterization of aerosol hygroscopicity, mixing state, and CCN activity at a suburban
663   site   in   the   central   North   China   Plain,   Atmos.   Chem.   Phys.,   18,   11739-11752,
664   https://doi.org/10.5194/acp-18-11739-2018, 2018.

665   Wehner, B., Birmili, W., Ditas, F., Wu, Z., Hu, M., Liu, X., Mao, J., Sugimoto, N., and Wiedensohler,
666   A.: Relationships between sub micrometer particulate air pollution and air mass history in Beijing,
667   China, 2004–2006, Atmos. Chem. Phys., 8, 6155–6168, https://doi.org/10.5194/acp-8-6155-2008,

668   2008.

669   Wexler, A.S., Clegg, S.L.: Atmospheric aerosol models for systems including the ions H$^+$, NH$_4^+$, Na$^+$,

670   SO$_4^{2-}$, NO$_3^-$, Cl$^-$, Br$^-$, and H$_2$O, J. Geophys. Res.-Atmos., 107 (D14): 14-14,

671   https://doi.org/10.1029/2001JD000451, 2002.

672   Whitby, K. T.: The physical characteristics of sulfur aerosols, Atmos. Environ., 12, 135–159,

673   https://doi.org/10.1016/j.atmosenv.2007.10.057, 1978.

674   Wiedensohler A.: An approximation of the bipolar charge distribution for particles in the submicron

675   size range, J. Aerosol Sci., 19, 387–389, https://doi.org/10.1016/0021-8502(88)90278-9, 1988.

676   Wu, G. X., Li, Z. Q., Fu, C. B., Zhang, X. Y., Zhang, R. Y., Zhang, R. H., Zhou, T. J., Li, J. P., Li, J.

677   D., and Zhou, D. G.: Advances in studying interactions between aerosols and monsoon in China,

678   Science China Earth Science, 59, 1–16, https://doi.org/10.1007/s11430-015-5198-z, 2016.

679   Wu, Z., Wang, Y., Tan, T., Zhu, Y., Li, M., & Shang, D., et al.: Aerosol liquid water driven by

680   anthropogenic inorganic salts: implying its key role in the haze formation over north china

681   plain, Environ. Sci. Technol. Lett., 5(3), 160-166, https://doi.org/10.1021/acs.estlett.8b00021, 2018.

682   Xu, L., Guo, H., Boyd, C. M., Klein, M., Bougiatioti, A., Cerully, K. M., Hite, J. R., Isaacman-

683   VanWertz, G., Kreisberg, N. M., Knote, C., Olson, K., Koss, A., Goldstein, A. H., Hering, S. V., de

684   Gouw, J., Baumann, K., Lee, S.-H., Nenes, A., Weber, R. J., and Ng, N. L.: Effects of anthropogenic

685   emissions on aerosol formation fromisoprene and monoterpenes in the southeastern United States,

686   P. Natl. Acad. Sci., 112, 37–42, https://doi.org/10.1073/pnas.1417609112, 2015.

687   Xu, W., Han, T., Du, W., Wang, Q., Chen, C., Zhao, J., Zhang, Y., Li, J., Fu, P., Wang, Z., Worsnop, D.

688   R., Sun, Y.: Effects of Aqueous- Phase and Photochemical Processing on Secondary Organic

689   Aerosol Formation and Evolution in Beijing, China, Environ. Sci. Technol. Lett., 51 (2), 762−770,

690   https://doi.org/10.1021/acs.est.6b04498, 2017.

691   Zheng, B., Zhang, Q., Zhang, Y., He, K. B., Wang, K., Zheng, G. J., Duan, F. K., Ma, Y. L., Kimoto,

692   T.: Heterogeneous chemistry: a mechanism missing in current models to explain secondary

693   inorganic aerosol formation during the January 2013 haze episode in North China, Atmos. Chem.

694   Phys., 15 (4), 2031−2049, https://doi.org/10.5194/acp-15-2031-2015, 2015.

695   Zieger, P., Väisänen, O., Corbin, J. C., Partridge, D. G., Bastelberger, S., Mousavi-Fard, M., Rosati,

696   B., Gysel, M., Krieger, U. K., Leck, C., Nenes, A., Riipinen, I., Virtanen, A., and Salter, M. E.:

697   Revising the hygroscopicity of inorganic sea salt particles, Nature communications, 8, 15883,

698   https://doi.org/10.1038/ncomms15883, 2017.

699

700
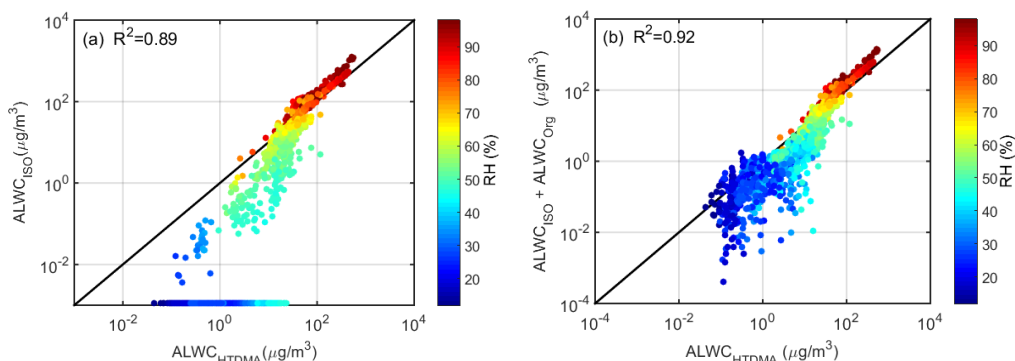
Figure 1. Comparison between ALWC$_{HTDMA}$ and (a) ALWC$_{ISO}$ and (b) the sum of ALWC$_{ISO}$ and ALWC$_{Org}$. ALWC$_{HTDMA}$ refers to calculated ALWC based on the measured growth factor and PNSDs, ALWC$_{ISO}$ refers to simulated ALWC from the ISORROPIA II model, and ALWC$_{Org}$ refers to the inferred ALWC contributed by organic species. The coefficient of determination R^2 is given in each panel. The color of the dots denotes the ambient RH; the solid line denotes the 1:1 line.
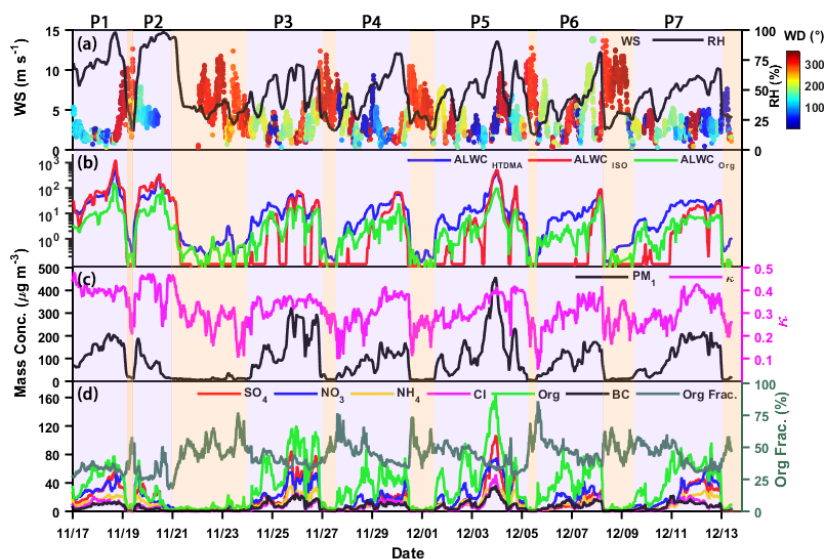
Figure 2. Time series of (a) wind speed (WS, left y-axis), ambient relative humidity (RH, right y-axis), and wind direction (WD, colored dots), (b) ALWC$_{HTDMA}$ (in blue), ALWC$_{ISO}$ (in red), and ALWC$_{Org}$ (in green), (c) PM$_1$ mass concentration (left y-axis) and hygroscopicity parameter (κ, right y-axis) calculated using the ZSR model described by Eq. (7), and (d) mass concentrations of aerosol species in PM$_1$ (left y-axis) and organic aerosol mass fraction

713   **(right y-axis). Seven polluted episodes (segments of the time series with a purple background) are selected for**

714   **examination.**

715
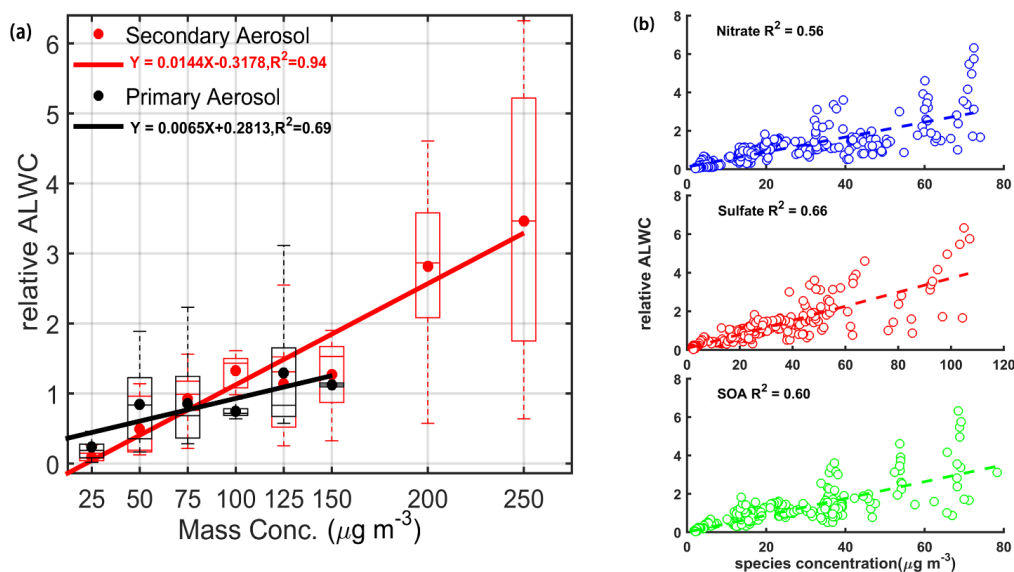
716

717   **Figure 3. The correlation analysis between relative ALWC and (a) primary (in black) and secondary (in red) aerosol**

718   **mass concentrations, and (b) nitrate, sulfate, and secondary organic aerosol (SOA) mass concentrations. Panel (a)**

719   **shows mean relative ALWCs (solid dots) with boxes showing the 25th, 50th, and 75th percentiles. The extremities**

720   **show the 5th and 95th percentiles. The solid lines in (a) and the dashed lines in (b) both represent the corresponding**

721   **best-fit lines from linear regression.**

722
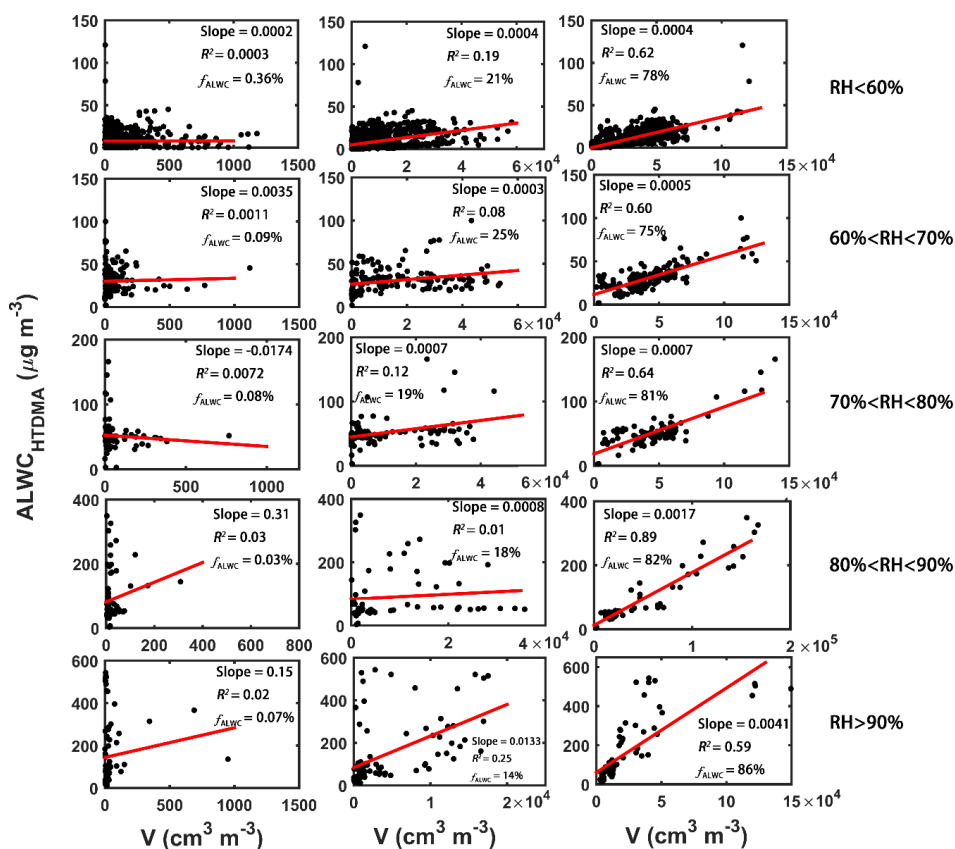
Figure 4. The correlation analysis between ALWC$_{HTDMA}$ and the volume concentration of nucleation mode (left column), Aitken mode (middle column), and accumulation mode (right column) particles under different ambient relative humidity (RH) conditions. The average contribution of each mode particles to ALWC under different ambient RH conditions is denoted by f_{ALWC}. The red lines represent the best-fit lines from linear regression.

729
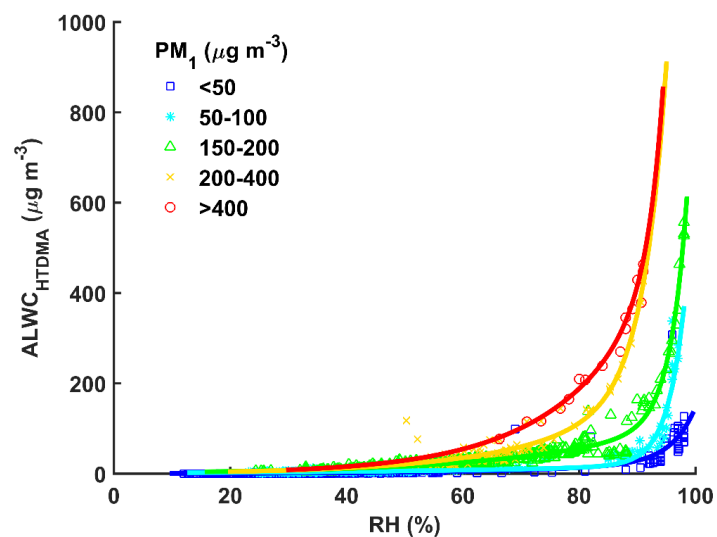
Figure 5. The dots show how ALWC$_{HTDMA}$ varies with the ambient relative humidity (RH) for different PM$_1$ mass

concentration ranges (colored symbols). The colored curves represent the best-fit lines through the data using the

fitting function $y = ae^{bx}$.

733

734
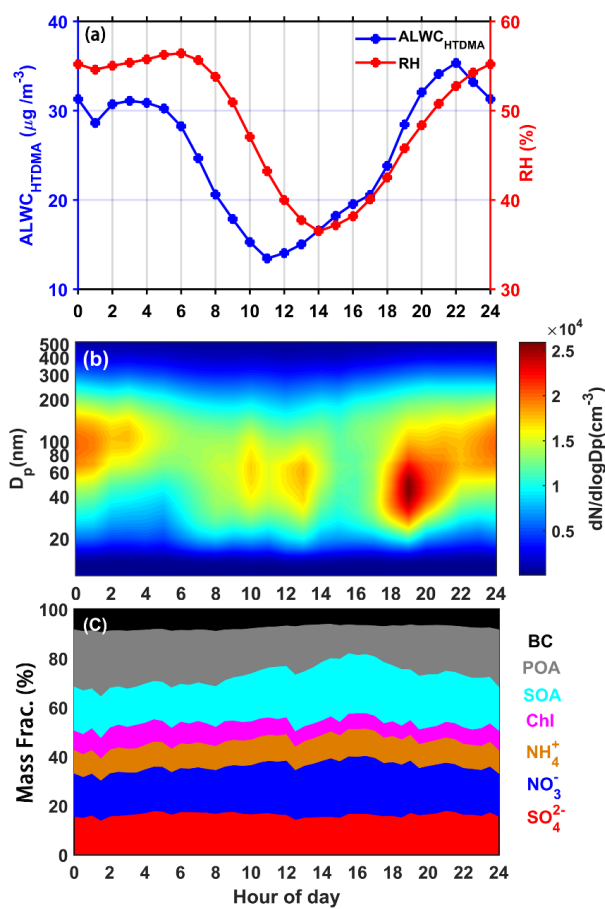
Figure 6. Diurnal variations of (a) ALWC$_{HTDMA}$ (in blue) and ambient RH (in red), (b) particle number size

distribution, and (c) the mass fraction of different chemical species. The time is in Beijing time.

737

738
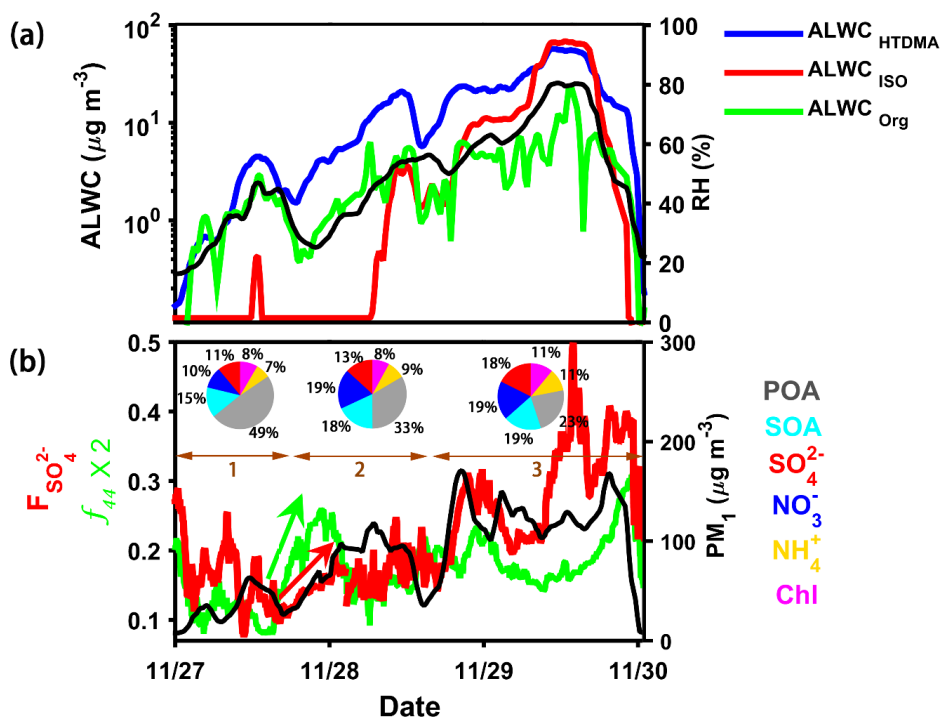
Figure 7. Time series of (a) $ALWC_{HTDMA}$ (in blue), $ALWC_{ISO}$ (in red), $ALWC_{Org}$ (in green), and RH (right y-axis), and

(b) the sulfur oxidation ratio ($F_{SO4^{2-}}$), f_{44}, and PM_1 mass concentration (right y-axis) during the P4 case in Figure 2.

The pie charts in (b) represent the average chemical compositions of PM_1 during three stages of the pollution event

(denoted by brown horizontal lines). The red and green arrows in (b) indicate the rapid increase in $F_{SO4^{2-}}$ and f_{44} at

the initial stage.

744